Sensors & Transducers
Published by IFSA Publishing, S. L., 2022
http://www.sensorsportal.com

Plasmonic Purcell Effect in Single Confined Metallic Layer

Cam Nhung VU and * Julien LAVERDANT
Institut Lumière Matière, Université Claude Bernard Lyon 1, CNRS,
Université de Lyon, F-69622 Villeurbanne, France
E-mail: julien.laverdant@univ-lyon1.fr

Received: 26 November 2021 /Accepted: 29 December 2021 /Published: 31 January 2022

Abstract: In this paper, we present a theoretical and simulation work about the modification of the spontaneous emission of a radiating dipole into a plasmonic device. This problem concerns devices where a nanolight source is directly integrated in nanophotonic devices. The modification of radiation, also called Purcell effect, is calculated using electromagnetism theory of the dissipated power of a point source near or inside a multilayer system. After describing the general effect and the theoretical approach based on the calculation of the Local Density of Optical States (LDOS), we present how this dipole radiates near a metal mirror which supports Surface Plasmon Polariton (SPP) at the metal-dielectric interface. In a second step, we set our attention onto a symmetric system where the metallic layer is confined between 2 insulators. In that late case, the SPP at each interface hybridize to generate two new modes named Long-Range and Short-Range Plasmon. In particular, we analyze the coupling efficiency of the dipole into these new modes and discuss about some potential applications in nanophotonics. The last part of this paper deals with a more realistic device where the insulator layers display finite sizes which lead to the existence of waveguided mode in the structure.

Keywords: Purcell effect, Surface plasmon, Waveguide, Strong coupling, Mode hybridization, Coupling efficiency, Nanophotonic.

1. Introduction

Among the numerous developments in integrated photonic devices, there is still challenges to engineer more efficient nanosources of light [1]. The recent advances in nanofabrication have made possible the realization of optical telecommunication devices with many integrated specificities [2]. Nowadays, there is a strong demand on the development of integrated photonic quantum devices [3]. The light-matter interaction can be engineered to create: new lasers based on polariton condensates [4], polariton fluids [5], single photon sources [6], reconfigurable photonic elements that can be switched [7], low loss waveguides [8], quantum logical gates [9], generation of non-classical state of light [10], wavelength conversion and non-linearities [11]. All these promising applications rely on the design of integrated devices that are compact, efficient without losses. In general, much materials depend on the wavelength of applications either by their optical dispersion or absorption, bands diagram, direct or indirect gap [12].

For example, vertical devices based on Bragg mirrors with a micro-cavity have been designed to realize semiconductor lasers [13] or ultra-bright single-photon sources [14]. The idea of this 1D photonic crystal has been extended to 2D photonic crystals [15]. Many realizations for quantum optics have been achieved based on these photonic crystals such as waveguided single photon sources [16], strong coupling [17], polarization entanglement [18] and ultrafast lasers [19]. The key point in all these realizations is the optimization of the devices. One criteria, to optimize the light-matter interaction, is based on the Purcell factor [20] that stipulates that the photon emission rate is increased when the emitter is inserted in a device with a confined mode volume and a strong quality mode factor. The mode volume is in general diffraction limited [21]. The quality factor that represent the time of interaction between the photon and the mode depends strongly on the losses inside the device [22]. For example, in the case of a nano-cavity inserted inside a photonic crystal, the cavity-edges are crucial [22, 23]. In this case, losses are induced by the junction between the cavity field and the mirror which lead to evanescent lossy waves.

Otherwise, evanescent waves can present advantages due to a high confinement of the mode volume which is smaller than the diffraction limit [24]. In the case of metals, Surface Plasmon Polaritons (SPPs) are evanescent waves at the interface between a metal and a dielectric interface [25]. SPPs are electromagnetic waves that propagate over a few microns at the metal-dielectric interface. It is an evanescent wave that possess a TM (or p) polarization. It is characterized by an in-plane wavevector given by Eq. (1) as:

$$k_{spp} = \frac{2\pi}{\lambda}\sqrt{\frac{\varepsilon_d \varepsilon_m}{\varepsilon_d + \varepsilon_m}}, \tag{1}$$

where λ is the wavelength and the dielectric constants of the dielectric and metal are respectively ε_d and ε_m. The dielectric constant of the metal is subject to losses so that the imaginary part can be important depending on the wavelength. Metals such as gold and silver are commonly used because they display few losses in the visible range [26]. As the dielectric constant, depends on the wavelength, the real part of the wavevector describe the dispersion relationship and the imaginary part is related to the propagation length L_{spp} [25].

Despite their losses, the high confinement and strong associated electromagnetic field have led to many interesting applications. Stimulated emission in waveguide [27], vertical lasers based on TAMM mode [28] and nano-lasers also called SPASER [29] have been demonstrated. Quantum plasmonic has emerged and demonstrations such as strong coupling [30, 31], single plasmons [32] and coalescence [33, 34] have been realized. Recently collective emission in superradiant state induced by SPP have been achieved [35].

Nevertheless, the major limitations of SPP come from the losses form the optical constant or by leakage. In the case of a thin metallic layer, the SPP mode can be leaky so that the propagation length is reduced. There is a particular case when the metallic layer is very thin and inserted between 2 identical insulators. The plasmon at each interface hybridize into a long-range and a short range plasmon [36, 37]. The long-range mode possesses a propagation length a few times higher than the SPP and is particularly interesting for integrated devices such as waveguides [38] and interferometers [39]. A demonstration of strong coupling for quantum optics has also been achieved [40].

The motivation of the present work is to show how quantum emitters (such as single molecule or quantum dots) can couple to a planar metallic layer that support hybridized SPP and in particular to realistic structures composed of finite size layers. This fundamental case is particularly important for integrated nanosources or quantum plasmonic with surface plasmons.

In a first part, we recall and detail how we calculate the Local Density of Optical States to deduce the Purcell factor. In a second step, we apply the model to the case of a gold mirror to identify and recall the coupling properties to a Surface Plasmon. In the two last part of the paper, we discuss the cases when the metallic layer is thin and inserted between insulators. The case of infinite insulating layers will be discussed to identify the modes and understand the coupling. A second case will be discussed which is more realistic when the insulators possess finite sizes.

2. Theoretical Model for the Calculation of the Purcell Effect and the LDOS

2.1. Link Between the Local Density of Optical States (LDOS) and the Purcell Factor

The spontaneous decay rate of a two level system weakly coupled to an external electromagnetic mode follows the Fermi's golden rule:

$$\Gamma = \frac{\omega\pi}{3\varepsilon_0\hbar}|p|^2 \rho(r,\omega), \tag{2}$$

where the Local Density of Optical States (LDOS) is ρ, the amplitude and the position of the dipole are respectively $|p|^2$ and r. The ratio of the decay rate of the 2-level system in a local (Γ) and a homogeneous surrounding (Γ_0) has been introduced by Purcell [20]:

$$F_p = \frac{\Gamma}{\Gamma_0} = \frac{\rho}{\rho_0} \tag{3}$$

The Purcell factor represents at the same time the modification of the decay rate and the LDOS. The published work [20] shows that the spontaneous decay rate of a single emitter was modified when placed inside a Fabry-Perot cavity. In such cavity, the emitter will decay in modes described by successive lorentzian functions of the frequency. It has been demonstrated that the modification follows:

$$F_P = \frac{3\lambda^3}{4\pi^2}\frac{Q}{V}, \tag{4}$$

where F_p is the so-called Purcell factor, λ is the emission wavelength of the emitters, Q and V are characteristics of the mode. Q is the resonance quality factor and V is the mode volume defined, in a non-dispersive medium of local optical constant $\varepsilon(r)$, as:

$$V = \frac{\int \varepsilon(r)\left|E(r)\right|^2 dr}{\max[\varepsilon(r)\left|E(r)\right|^2]} \tag{5}$$

In this expression, $|E(r)|^2$ is the intensity of the electric field associated to the mode. The final expression of the Purcell factor in Eq. (4) shows that it is maximum when the quality factor is very high and the mode volume is small. In the case considered in this paper, we use plasmonic structures based on metals so that the quality factor will be generally under 100 but the field confinement possesses a mode volume smaller than λ^3.

2.2. Power Dissipation of a Dipole Near a Planar Structure

The general Purcell factor is defined by Eq. (3) which is the ratio of the decay rates. In principle, the decay rates can only be calculated in quantum mechanics and differ from classical formula. Nevertheless, the relative modifications of the emission rates in presence of a nanostructured compared to free space are identical [41].

$$F_p = \left(\frac{\Gamma}{\Gamma_0}\right)_{quantum} = \left(\frac{\Gamma}{\Gamma_0}\right)_{classic} \tag{6}$$

Using this analogy, we are able to use classic electromagnetism calculations to simulate the Purcell factor. For that model, we consider the power P dissipated by a dipole of energy E_{dipole}:

$$P = -\Gamma E_{dipole} \tag{7}$$

In the present work, we consider surface modes which are defined by their in-plane wavevector $k_{//}$. In the following, we will use the normalized wavevector u such as:

$$u = n_0 \frac{k_{//}}{2\pi / \lambda}, \tag{8}$$

where n_0 is the optical index where the dipole is located, u is very interesting parameters that delimits propagating waves in free space ($u<n_0$) and evanescent waves ($u>n_0$). Furthermore, by this definition, u will also represent the effective index of the modes. The Purcell factor can be therefore decomposed on these wavevectors by [42]:

$$F_p = \int \alpha(u) du \tag{9}$$

The quantity α represents the derivative of the power dissipated by wavevector and will allow us to identify surface modes. The expression of α depends on the position of the dipole and its orientation. In Fig. 1, we present the two main cases that are considered. The dipole is placed in the medium 0. The emitted electromagnetic waves will depend on the orientation of the dipole. If the dipole is parallel to the surface, TM (p) and TE (s) waves will excite the surface. In the case of a vertical dipole, only TM (p) waves will be generated [41]. As this paper deals with the excitation of SPP which are TM (p) modes, we set the dipole vertical to the all interfaces.

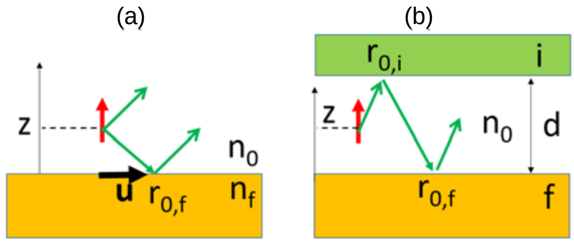

Fig. 1. Schematic of the calculated system. The dipole (red arrow) is set at a distance z from the bottom interface. (a) Dipole placed inside a semi-infinite medium, and (b) inside a layer of thickness d. 0, i and f denotes the dipole medium, upper and bottom layer respectively. Note that the medium i or f can be composed of multilayers.

The general expression of α for a vertical dipole (orientation perpendicular to the layer) is:

$$\alpha_\perp(u) = \frac{3}{2}\mathrm{Re}\left[1 + g(u)\frac{u^3}{\sqrt{n_0^2 - u^2}}\right] \tag{10}$$

In this expression, we observe two terms which comes from the direct light in a direction u and a second one that depend on the function *g(u)*.

2.3. Analytic Expression of the Dissipated Power in a Multilayer Structure

As we see on the general expression of the dissipated power, we need the expressions of the function *g(u)*. Its formula is given by $g_1(u)$ or $g_2(u)$ if the dipole is placed in a semi-infinite layer (Fig. 1(a)) or inside a finite layer (Fig. 1(b)). For a single interface (Fig. 1(a)), the expression is given by [42]:

$$g_1(u) = r_{0,f}^p \exp(2ik_{z,0}z) \tag{11}$$

The projection of the wavevector is $k_{z,0} = \frac{2\pi}{\lambda}\sqrt{n_0^2 - u^2}$. We see that in the case of a semi-infinite layer, $g_1(u)$ is only given by the propagation distance to the interface and the Fresnel reflection coefficient $r_{0,f}^{p}$. If the dipole is placed inside a finite layer, we have:

$$g_2(u) = \frac{1}{1-2r_{0,f}^{p}r_{0,f}^{p}\exp(2ik_{z,0}d)} \{2r_{0,i}^{p}r_{0,f}^{p}\exp[2ik_{z,0}d] + r_{0,i}^{p}\exp[2ik_{z,0}(d-z)] + r_{0,f}^{p}\exp(2ik_{z,0}z)\} \quad (12)$$

The main difference with one interface is that the reflection coefficient of both upper ($r_{0,i}^{p}$) and lower ($r_{0,f}^{p}$) layer must be taken into account. For clarity of the different expressions, we removed the angular dependence of the Fresnel coefficient with the in-plane wavevector u. Finally, the Fresnel reflection coefficients are calculated by analytical Matrix formalism [43] and depends on the considered structure through their indices and thicknesses.

2.4. Coupling Efficiency (β-factor)

So far, we have presented the Purcell factor that represents the modification of the total power of the emitter. It is also very useful to quantify the coupling efficiency in each available mode or channel. This parameter is a key point in the optimization of devices for integrated photonics as for example waveguides or cavities [16]. The coupling efficiency in a specific mode is called the β-factor and is defined as:

$$\beta = \frac{\Gamma_{mode}}{\Gamma_{total}} = \frac{\int_{u\in\{mode\}}\alpha(u)du}{\int_{0}^{+\infty}\alpha(u)du} \quad (13)$$

The β-factor will then be calculated using the value of the power α from the previous expression.

2.5. Reconstruction of the Mode Profile

It is also very useful to dispose of the shape of the mode profile in order to identify the modes and locate where the electromagnetic field is more intense. The last quantity, we can compute with the dissipated power α is the power in each mode:

$$\frac{\Gamma_{mode}}{\Gamma_0} = \int_{u\in\{mode\}}\alpha(u)du \quad (14)$$

This quantity is normalized and will represent the normalized power of the mode. For each position of the dipole, the dissipated power α is calculated and integrated. The profile of the mode will then be deduced. This procedure is a way to reconstruct the mode volume which is fundamental to understand the Purcell factor.

3. Spontaneous Emission of a Radiating Dipole near a Thick Gold Mirror

In the previous part, we described the model and defined the different physical quantities that we will calculate. We first consider the simple case of a dipole coupled to a gold mirror [48]. For the calculation, we set the dipole emission wavelength λ=650nm so that the gold optical index is [26]: n_{gold}=0.15+3.32i. The results are presented in Fig. 2.

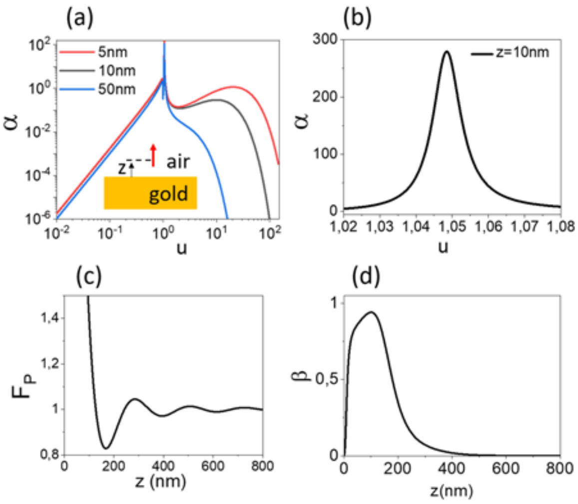

Fig. 2. Simulations of the power dissipated by a vertical dipole in the air located near a gold mirror. (a) Dissipated power as function of u for several gold-dipole distance; (b) Zoom of the dissipated power (for z=10 nm) around the plasmonic resonance u_{SPP}=1.048. (c) Evolution of the Purcell factor with the vertical distance z. (d) Coupling efficiency to the SPP mode as function of the distance.

When the dipole is near the gold mirror, we observe that the dissipated power is absorbed into 3 regions in Fig. 2 (a). When u<1, the power is radiated in free space whereas when u>1, the power is absorbed into the evanescent waves. It is known, that in the evanescent part, two modes arise which are the Surface Plasmon Polaritons with a wavevector defined by Eq. (1) and a broad range of wavevectors above the SPP which are called Lossy Surface Waves (LSW).

If we make a zoom to identify the shape of SPP in Fig. 2 (a), we clearly observe in Fig. 2 (b) a Lorentzian-type shape curve centered at u=1.048 which perfectly matches the value from Eq. (1). More information can be deduced from this curve. As it is well known [44], the SPP is a purely coherent mode so that it is only limited by Fourier Transform. Therefore, the width in wavevector (Δu) is related to the intensity decay length of the SPP (L_{SPP}). The relationship in the case of a Lorentzian-type shape is given by:

$$L_{SPP} = \frac{\lambda}{\pi\Delta u} \quad (15)$$

With the value deduced in Fig. 2 (b), we extract a propagation length of 20 µm. The Purcell factor presented in Fig. 2 (c) is decreasing with the distance z and then make a few oscillations around 1. As the distance z is increasing, the number of optical modes are decreasing. Oscillations appear from interferences of the light emitted by the dipole and its reflection. From the power, we extract the β-factor to the SPP as previously explained. In Fig. 2(d), the maximum efficiency that is found is around 90 % for a distance of 100 nm. This very high absorption into SPP comes from the vertical orientation of the dipole [45].

4. Purcell Effect near a Confined Gold Film: the Long-range Surface Plasmon

In the previous part, we discussed about the coupling of the dipole near a gold mirror. A gold mirror is a good approximation when the gold thickness is more than 5 times the skin depth of the metal [45]. In this part, we analyze the case of a gold film which size is similar to the skin depth. If we position the radiating dipole above the thin gold layer, a new plasmonic channel is opened. Indeed, the surface will now support one SPP on each interfaces [25]. This case becomes more interesting when the insulators surrounding the gold layer possess the same optical index as we will show in the following. In Fig. 3, we simulate the dissipated power of the dipole located in the glass above a thin gold layer (20 nm thick).

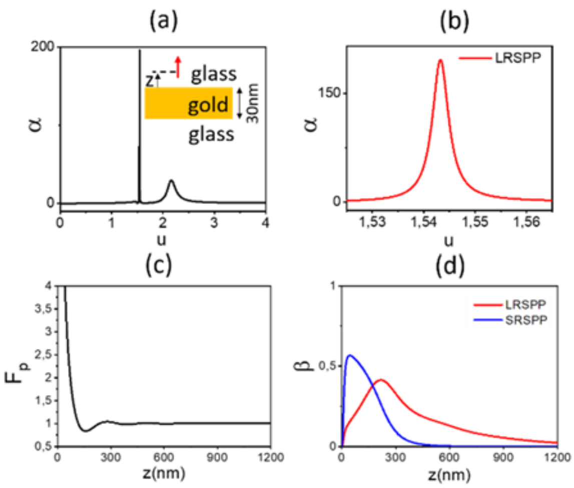

Fig. 3. Simulations of the power dissipated by a vertical dipole in the glass near a very thin gold layer. (a) Dissipated power as function of u for z=10 nm. (b) Zoom of the dissipated power around the LRSPP mode around u_{LRSPP}=1.544. (c) Evolution of the Purcell factor with the vertical distance z. (d) Coupling efficiency to the LRSPP and SRSPP modes as function of the distance.

When the optical indices around the thin gold layer are the same, the SPP on each side possesses the same momentum so that SPP hybridization occurs [36]. This phenomenon is similar to the case of bonding and antibonding of the wave functions in a molecular system or in strong coupling in quantum physics. As a consequence, two new SPPs arise: the long-range (LRSPP) and short-range (SRSPP) surface plasmons. In Fig. 3, we clearly observe that the dipole located at 10 nm from this surface excite these two modes with different width Δu. From Fig. 3(a), we identify the mode with smaller width (located at u=1.544) to the long-range plasmon whereas the other mode (at u=2.16) is called the short range plasmon. It is important to highlight that a strong width reduction occurs for the case of long-range as presented in Fig. 3(b). From the width in u, we deduce that the propagation length of the long-range and short range plasmon are respectively 100 µm and 1 µm. The evolution of the Purcell factor in Fig. 3(c) is very similar to the one in the case of the gold mirror in Fig. 2(c). Indeed, the device does not create new modes but split the initial mode in 2 but with different amplitudes. This last observation is also valid for the coupling efficiencies presented in Fig. 3(d). The short range plasmon is located at very small distance to the interface (42 nm) with a maximum efficiency of 56 % whereas the long-range plasmon maximum efficiency is around 42 % for a distance farther to the interface (225 nm).

For many applications which need a longer propagation constant such as integrated interferometers for example, the long-range mode is particularly interesting. This mode has the same properties of the SPP (same Purcell factor) and propagates 5 times farther. Nevertheless, the maximum coupling efficiency is only 42 % at maximum.

5. Coupling a Dipole to a Finite Gold Film Deposited Onto a Glass Substrate

In this last part, we focus on a realistic device with finite size layers surrounding the thin gold film. We will describe how to optimize the structure depending on the purpose of the desired applications. The whole structure is deposited on a prism of higher index to allow the extraction of the plasmon mode. This experimental scheme is also called the Otto configuration [25, 46].

5.1. Schematic of a Realistic Device

In order to clarify the design of the multilayer structure, we display, in Fig. 4, a scheme of the modeled structure. We set a prism of high optical index (n=1.8) which can be made with LaSF glass with low absorbance for the visible wavelength [40]. The gold layer has a thickness of 30 nm and is sandwiched between two glass layers (n=1.5) of thickness 750 nm. The glass layer above the prism is denoted the coupling layer as it sticks the gold and the prism. The top glass layer will be called the cladding layer. The whole device is set in the air.

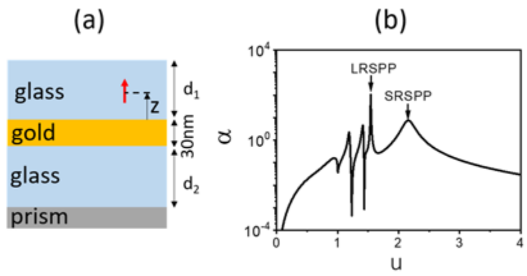

Fig. 4. (a) Schematic of the device under consideration. The dipole (red arrow) is placed in the upper glass at a distance z from the gold. The gold layer thickness is 20 nm and the glass thicknesses are respectively d_1=750 nm and d_2=750 nm for the top and bottom. The prism is semi-infinite. (b) Dissipated power α of the dipole at z=10 nm.

We also present in Fig. 4(b), a first calculation of the power dissipated by the dipole placed at 10 nm above the gold inside the top layer. The situation is the same as in Fig. 3 except that the glass possesses finite size. The result shows that complimentary to the 2 previously identified plasmonic modes (long-range and short-range), new modes appear at smaller wavevectors u. The wavevector of these modes lies between the air (u=1) and the glass (u=1.5). This particular case is very similar to the presence of waveguided modes in which the effective index of these modes lies in the interval between the optical index of the outside and the optical index of the internal part of the guide [47].

In order to validate the hypothesis of the appearance of waveguided modes and to highlight the dependence of these modes onto the parameters of the device, we present some calculation to optimize the modal structure.

5.2. Structure Optimization

The number of variable parameters become more important in the device's scheme of Fig. 4(a). We present in Fig. 5, a complimentary simulation. As explained in the description of our model, we need to calculate the Fresnel reflection coefficients. In the case under investigation in Fig. 4(a), we calculate the reflection coefficient R_p (in power) as function of the cladding layer (d_1) for different incident wavevector u. In this prism configuration, the incident angle θ is defined as: u=n sin(θ). The light is sent through the prism of index n=1.8. This light is propagative so that the maximum in-plane wavevector u is 1.8. The coupling layer (d_2) is fixed with a value d_2=750 nm.

In Fig. 5, we clearly identify the LRSPP which is located above u=1.5 and the WGM which are located for u in the interval [1-1.5]. This result shows that depending on the chosen thickness d_1, the number of guided modes change. One particularly interesting point is that the wavevector of the WGMs change with the thickness. As u also represents the effective index of the mode, we see that when d_1 is increasing, the effective index of the WGMs tends 1.5 which is the optical index of the glass.

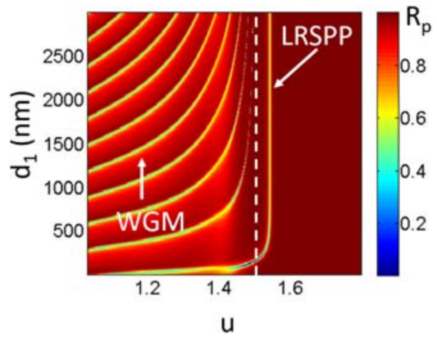

Fig. 5. (a) Evolution of the reflected intensity R_p as function of d_1 and u in an Otto-prism configuration. WGM: WaveGuided Modes. LRSPP: LongRange Surface Plasmon Polariton. The vertical white dashed line represents u=1.5.

As this map is useful to design devices with controlled number of modes for future applications, we give an example. If we take a cladding thickness of d_1=750 nm, we cross 2 WGMs and the LRSPP. This case corresponds to the result obtained in Fig. 4 when the dipole, inserted inside the device, has excited 2 WGMs, the long-range and short-range plasmons. The profiles of the different modes of this device are also reconstructed as explained by Eq. (14) and displayed in Fig. 6 as function of the vertical distance z within the device.

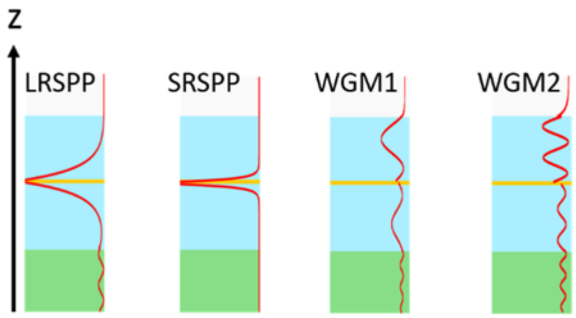

Fig. 6. Mode profiles (continuous red line) of the 4 modes available. The green, blue and yellow layers represent respectively the prism, the glass and the gold.

The profile of each mode is in good agreement with the previous analysis. The plasmonic modes (LRSPP and SRSPP) display exponential decays from the gold layer whereas the WGM present oscillations according to their order. Due to the symmetry of the device, the fundamental modes WGM1 is not exactly centered in the middle of the dielectric. Oscillations are also observed in the lower dielectric (coupling layer).

5.3. Influence of the Waveguided Modes on the Purcell Factor and Coupling Efficiencies

In the previous sub-part, we have presented how to optimize the number of waveguided modes in the final device by analyzing the evolution of the Fresnel reflection coefficient with the device parameters. We keep the same conditions $d_1=d_2=750$ nm in order to excite 2 waveguided modes (WGMs), the short-range (SRSPP) and long-range plasmon (LRSPP). Fig. 7 presents the Purcell factor and β-factors for this optimized structure as function of z for a vertical dipole located inside the cladding layer. Each mode's wavevector u has been identified in the dissipated power α(u), in Fig. 4 (b), and the coupling efficiency is then calculated with Eq. (13).

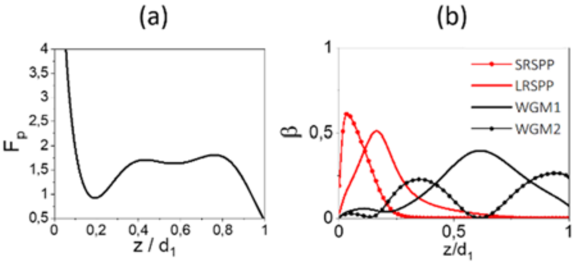

Fig. 7. (a) Purcell factor and (b) β-factors as a function of dipole-gold distance z normalized to the cladding thickness d_1=750 nm. The acronyms SRSPP, LRSPP and WGM are defined in the text.

The curve of the evolution of the Purcell factor in Fig. 7(a) is different than the previous one of Fig. 3(c). For small distances ($z<0.2d_1$), we observe the same evolution if the layers are infinite. Indeed, at small distances, the evanescent waves are not perturbed by the finite thickness (d_1=750 nm) so that the LDOS in this region is the same. An increase is observed for higher distances to the gold. Indeed, in this device, waveguided modes appear due to the presence of finite glass layers. These modes are propagative and are more located in the center of the dielectric as presented in Fig. 6. Therefore, we observe an increase of the LDOS around the middle of glass layer.

The coupling efficiencies to the long-range and short range plasmon in Fig. 7(b) are not modified. These are evanescent waves linked to the gold layer and are not perturbed by the presence of the waveguided modes. As previously explained, we have optimized this device to possess 2 WGMs. The optimal coupling distance to each mode depends on its order as seen in Fig. 7(b). For example, the fundamental guided mode (WGM1) is nearly centered inside the glass layer. Note that the asymmetry of WGM comes from geometry of the device. Finally, in this particular example, the coupling efficiency to WGM1 is around 40 % which is similar to the β of the LRSPP.

6. Conclusion

In this paper, we have presented the model to calculate the modification of the spontaneous emission of a dipole near multi-layer structures. The radiated emission is characterized by the Purcell factor and the coupling efficiency to the desired optical modes. In the case of plasmonic structures, the Purcell factor can be important at very short distance due to an important density of optical states. Nevertheless, all the emission will be dissipated in lossy modes. A compromise can be found with the coupling distance where the Purcell factor is still important and the emission is efficiently coupled to the desired mode without too important losses.

In particular, we focused our work onto the Surface Plasmon Polaritons excited on a gold mirror or a thin gold layer between insulators. In the late case, new plasmons arise from the coupling between each interface. A specific mode called the long-range plasmon can be excited with nearly 50 % of efficiency which possess a propagation length of 100 µm for visible wavelengths. At the end, we presented a realistic structure composed of finite size layers deposited on a substrate. In this case, new optical modes appear from the insulators. We have shown that these new modes are waveguided waves. We presented an optimization of the structure in order to control the number of waveguided modes available for the dipole. This particular case is very promising for integrated nanophotonic devices as it possesses many modes linked to the metal or the insulator with propagation length of a few 100 µm.

Acknowledgements

The authors acknowledge the French region Auvergne-Rhône-Alpes (PAI n° 21PACK-LAV).

References

[1]. V. P. Veiko, V. I. Konov, Fundamentals of Laser-Assisted Micro- and Nanotechnologies, *Springer Series in Material Sciences*, Springer, Vol. 195, 2014.

[2]. H. Zhang, M. Gu, X. D. Jiang, J. Thompson, H. Cai, S. Paesani, R. Santagati, A. Laing, Y. Zhang, M. H. Yung, Y. Z. Shi, F. K. Muhammad, G. Q. Lo, X. S. Lo, B. Dong, D. L. Kwong, L. C. Kwek, A. Q. Liu, An optical neural chip for implementing complex-valued neural network, *Nature Communication*, Vol. 12, 2021, 457.

[3]. A. W. Elshaari, W. Pernice, K. Srinivasan, O. Benson and V. Zwiller, Hybrid integrated quantum photonic circuits, *Nature Photonics*, Vol. 14, Issue 5, 2020, pp. 285-298.

[4]. E. Wertz, L. Ferrier, D. D. Solnyshkov, R. Johne, D. Sanvitto, A. Lemaître, I. Sagnes, R. Grousson, A. V. Kavokin, P. Senellart, G. Malpuech, J. Bloch, Spontaneous formation and manipulation of extended polariton condensates, *Nature Physics*, Vol. 6, Issue 11, 2010, pp. 860-864.

[5]. A. Amo, S. Pigeon, D. Sanvitto, G. G. Sala, R. Hivet, I. Carusotto, F. Pisanello, G. Leménager, R. Houdré, E. Giacobino, C. Ciuti, A. Bramati, Polariton Superfluids Reveal Quantum Hydrodynamic Solitons, *Science*, Vol. 332, Issue 6034, 2011, pp. 1167-1170.

[6]. E. Meyer-Scott, C. Silberhorn, A. Migdall, Single-photon sources: Approaching the ideal through multiplexing, *Review of Scientific Instruments*, Vol. 91, Issue 4, 2020, 041101.

[7]. B. J. Metcalf, J. B. Spring, P. C. Humphreys, N. Thomas-Barbieri, W. S. Kolthammer, X.-M. Jin, N. K. Langford, D. Kundys, J. C. Gates, B. J. Smith, P. G. R. Smith, I. A. Walmsley, Quantum teleportation on a photonic chip, *Nature Photonics*, Vol. 8, 2014, pp. 770-774.

[8]. A. Politi, J. C. F. Matthews, M. G. Thompson, J. L. O'Brien, Integrated Quantum Photonics, *IEEE Journal of Selected Topics in Quantum Electronics,* Vol. 15, Issue 6, 2009, pp. 1673-1684.

[9]. Y. Zhou, D-Y. Lü, W-Y. Zeng, Chiral single photon switch-assisted quantum logic gate with a nitrogen-vacancy center in a hybrid system, *Photonic Research*, Vol. 9, Issue 3, 2021, 405.

[10]. S. Azzini, D. Grassani, M. J. Strain, M. Sorel, L. G. Helt, J. E. Sipe, M. Liscidini, M. Galli, D. Bajoni, Ultra-low power generation of twin photons in a compact silicon ring resonator, *Optics Express*, Vol. 20, Issue 21, 2012, pp. 23100-23107.

[11]. X. Guo, C-l. Zou, C. Schuck, H. Jung, R. Cheng, H. X. Tang, Parametric down-conversion photon-pair source on a nanophotonic chip, *Light: Science & Applications*, Vol. 6, Issue 5, 2017, e16249.

[12]. M. Fox, Optical Properties of Solids, Oxford Master Series in Condensed Matter Physics, *Oxford University Press*, 2010.

[13]. R. Michalzik, VCSELs: Fundamentals, technology and Applications of Vertical-Cavity Surface-Emitting lasers, *Springer Series in Optical Sciences, Springer*, 2013.

[14]. A. Dousse, L. Lanco, J. Suffczynski, E. Semenova, A. Miard, A. Lemaître, I. Sagnes, C. Robin, J. Bloch, P. Senellart, Controlled Light-Matter Coupling for a Single Quantum Dot Embedded in a Pillar Microcavity Using Far-Field Optical Lithography, *Physical Review Letters*, Vol. 101, Issue 26, 2008, 267404.

[15]. J. D. Joannopoulos, S. G. Johnson J. N. Winn, R. D. Meade, Photonic Crystals Molding the flow of Light, *Princeton University*, 2008.

[16]. H. Thyrrestrup, L. Sapienza, P. Lodahl, Extraction of the β-factor for single quantum dots coupled to a photonic crystal waveguide, *Applied Physics Letters*, Vol. 96, 2010, 231106.

[17]. M. A. Dundar, J. A. M. Voorbraak, R. Nötzel, A. Fiore, R. W. Van der Heijden, Multimodal strong coupling of photonic crystal cavities of dis-similar size, *Applied Physics Letters*, Vol. 100, 2012, 081107.

[18]. G. He, C. Zhu, Y. Jiang, J. Ren, Y. Guo, J. Jing, Generation of path-polarization hyper entanglement using quasi-phase-matching in quasi-periodic non-linear photonic crystal, *Scientific Reports*, Vol. 7, 2017, 4954.

[19]. H. Altug, D. Englund, J. Vuckovic, Ultrafast photonic crystal nanocavity laser, *Nature Physics*, Vol. 2, 2006, pp. 484-488.

[20]. E. M. Purcell, Spontaneous Emission Probabilities at Radio Frequencies, *Physical Review*, Vol. 69, 1946, 681.

[21]. G. Grynberg, A. Aspect, C. Fabre, Introduction to quantum optics, *Cambridge University Press*, 2010.

[22]. P. Lalanne, C. Sauvan, J. P. Hugonin, Photon confinement in photonic crystal nanocavities, *Laser & Photonics Reviews*, Vol. 2, Issue 6, 2008, pp. 514-526.

[23]. Y. Akahane, T. Asano, B-S. Song, S. Noda, High-Q photonic nanocavity in a two-dimensional photonic crystal, *Nature*, Vol. 425, 2003, pp. 944-947.

[24]. A. F. Koenderink, On the use of Purcell factors for plasmon antennas, Optics Letters, Vol. 35, Issue 24, 2010, pp. 4208-4210.

[25]. S. A. Maier, Plasmonics: Fundamentals and Applications, *Springer*, 2007.

[26]. P. B. Johnson, R. W. Christy, Optical Constants of the Noble Metals, *Physical Review B*, Vol. 6, Issue 12, 1972, pp. 4370-4379.

[27]. J. Grandidier, G. Colas des Francs, S. Massenot, A. Bouhelier, L. Markey, J.-C. Weeber, C. Finot, A. Dereux, Gain-Assisted Propagation in a Plasmonic Waveguide at Telecom Wavelength, *Nanoletters*, Vol. 9, Issue 8, 2009, pp. 2935-2939.

[28]. C. Symonds, G. Lheureux, J. P. Hugonin, J. J. Greffet, J. Laverdant, G. Brucoli, A. Lemaître, P. Senellart, J. Bellessa, Confined Tamm Plasmon Lasers, *Nano Letters*, Vol. 13, Issue 7, 2013, pp. 3179-3184.

[29]. R.-M. Ma, R. F. Oulton, Applications of nanolasers, *Nature Nanotechnology*, 14, Issue 1, 2019, pp. 12-22.

[30]. P. Törma, W. L. Barnes, Strong coupling between surface plasmon polaritons and emitters: a review, *Reports on Progress in Physics*, Vol. 78, Issue 1, 2015, 013901.

[31]. R. Chikkaraddy, B. de Nijs, F. Benz, S. J. Barrow, O. A. Scherman, E. Rosta, A. Demetriadou, P. Fox, O. Hess, J. J. Baumberg, Single-molecule strong coupling at room temperature in plasmonic nanocavities, *Nature*, 535, Issue 7610, 2016, pp. 127-130.

[32]. A. V. Akimov, A. Mukherjee, C. L. Yu, D. E. Chang, A. S. Zibrov, P. R. Hemmer, H. Park, M. D. Lukin, Generation of single optical plasmons in metallic nanowires coupled to quantum dots, *Nature*, Vol. 450, Issue 7168, 2007, pp. 402-406.

[33]. B. Vest, M.-C. Dheur, E. Devaux, A. Baron, E. Rousseau, J. P. Hugonin, J. J. Greffet, G. Messin, F. Marquier, Anti-coalescence of bosons on a lossy beam splitter, *Science*, Vol. 356, Issue 6345, 2017, pp. 1373-1376.

[34]. G. Fujii, T. Segawa, S. Mori, N. Namekata, D. Fukuda, S. Inoue, Preservation of photon indistinguishability after transmission through surface-plasmon-polariton waveguide, *Optics Letters*, Vol. 37, Issue 9, 2012, pp. 1535-1537.

[35]. Y. Luo, G. Chen, Y. Zhang, L. Zhang, Y. Yu, F. Kong, X. Tian, Y. Zhang, C. Shan, Y. Luo, J. Yang, V. Sandoghdar, Z. Dong, J. G. Hou, Electrically Driven Single-Photon Superradiance from Molecular Chains in a Plasmonic Nanocavity, *Physical Review Letters*, Vol. 122, Issue 23, 2019, 233901.

[36]. P. Berini, Long-range surface plasmon polariton, *Advanced Optics and Photonics*, Vol. 1, 2009, pp. 484-588.

[37]. J. Laverdant, C-N. Vu, Purcell factors of hybrid surface plasmons and waveguided modes, in *Proceeding of the 4th International Conference on Optics, Photonics and Lasers (OPAL'2021)*, Corfu, Greece, 13-15 October 2021, pp. 39-40.

[38]. A. Degiron, S.-Y. Cho, C. Harrison, N. M. Jokerst, C. Dellagiacoma, O. J. F. Marin, D. R. Smith, Experimental comparison between conventional and

hybrid long-range surface plasmon waveguide bends, *Physical Review A*, Vol. 77, Issue 2, 2008, 021804(R).
[39]. H. Fan, R. Charbonneau, P. Berini, Long-range surface plasmon triple-output Mach-Zehnder interferometers, *Optics Express*, Vol. 22, Issue 4, 2014, pp. 4006-4020.
[40]. K. Chevrier, J.-M. Benoit, C. Symonds, J. Paparone, J. Laverdant, J. Bellessa, Organic Excitons in strong coupling with long-range surface plasmons and waveguided modes, *ACS Photonics*, Vol. 5, Issue 1, 2018, pp. 80-84.
[41]. L. Novotny, B. Hecht, Principles of Nano-Optics, *Cambridge University Press*, 2006.
[42]. W. Lukosz, Theory of optical-environment-dependent spontaneous-emission rates for emitters in thin layers, *Physical Review B*, Vol. 22, 1980, pp. 3030-3038.
[43]. A. Shalabney, I. Abdulhalim, Electromagnetic fields distribution in multilayer thin film structures and the origin of sensitivity enhancement in surface plasmon resonance sensors, *Sensors and Actuators A: Physical*, Vol. 159, Issue 1, 2010, pp. 24-32.
[44]. S. Aberra Guebrou, J. Laverdant, C. Symonds, S. Vignoli, J. Bellessa, Spatial coherence properties of surface plasmon investigated by Young's slit experiment, *Optics Letters*, Vol. 37, Issue 11, 2012, pp. 2139-2141.
[45]. C. Vion, P. Spinicelli, L. Coolen, C. Schwob, J.-M. Frigerio, J.-P. Hermier, A. Maître, Controlled modi-fication of single colloidal CdSe/ZnS nanocrystal fluorescence through interactions with a gold surface, *Optics Express*, Vol. 18, Issue 7, 2010, pp. 7440-7455.
[46]. A. Otto, Excitation of nonradiative surface plasma waves in silver by the method of frustrated total reflection, *Zeitschrift Für Physik A: Hadrons Nuclei*, Vol. 216, Issue 4, 1968, pp. 398-410.
[47]. M. Born, E. Wolf, Principles of Optics, Electromagnetic Theory of Propagation Interference and Diffraction of Light, *Cambridge University Press*, 2005.
[48]. G. Colas des Francs, J. Barthes, A. Bouhelier, J. C. Weber, A. Dereux, A. Cuche, C. Girard, Plasmonic Purcell factor and coupling efficiency to surface plasmons. Implications for addressing and controlling optical nanosources, *Journal of Optics*, Vol. 18, Issue 9, 2016, 094005.

___